

Responses of a Tall Building in Los Angeles, California, as Inferred from Local and Distant Earthquakes

Mehmet Çelebi,^{a)} M.EERI, Hasan S. Ulusoy,^{b)} and Nori Nakata^{c)}

The increasing inventory of tall buildings in the United States and elsewhere may be subjected to motions generated by near and far seismic sources that cause long-period effects. Multiple sets of records that exhibited such effects were retrieved from tall buildings in Tokyo and Osaka ~350 km and 770 km, respectively, from the epicenter of the 2011 Tohoku earthquake. In California, very few tall buildings have been instrumented. An instrumented 52-story building in downtown Los Angeles recorded seven local and distant earthquakes. Spectral and system identification methods exhibit significant low frequencies of interest (~0.17 Hz, 0.56 Hz, and 1.05 Hz). These frequencies compare well with those computed by transfer functions; however, small variations are observed between the significant low frequencies for each of the seven earthquakes. The torsional and translational frequencies are very close and are coupled. Beating effect is observed in at least two of the seven earthquake data. [DOI: 10.1193/050515EQS065M]

INTRODUCTION

In many cities of the United States and other countries, new tall buildings with different architectural and structural features are being built. Many of the cities are expanding their inventories of tall buildings, which are affected by seismic waves that originate at near and far distant sources. On the other hand, among the vast majority of cases, very few seismic stations or arrays are available on the ground nearby (e.g., at distances less than twice the height of the buildings) or within the tall buildings.

In addition, many of the tall buildings (e.g., >50 stories) are built on geological basins (e.g., downtown Los Angeles and downtown San Francisco). As such, in general, local site conditions with low shear wave velocities and depths significantly shallower than basins do not adversely affect the responses of tall buildings, but basins and, particularly, deep basins can (e.g., the Los Angeles Basin). A detailed description and map of different basins in the Los Angeles area are provided by Hillhouse et al. (2012).

The purpose of this paper is to study records of an instrumented 52-story building in downtown Los Angeles, California. Figure 1 shows the location of the building on a map and a picture of the building. The map also shows locations of the epicenters of the seven

^{a)} Earthquake Science Center, USGS, Menlo Park, CA 94025

^{b)} Consulting Engineer, Palo Alto, CA

^{c)} Stanford University, Stanford, CA 94305

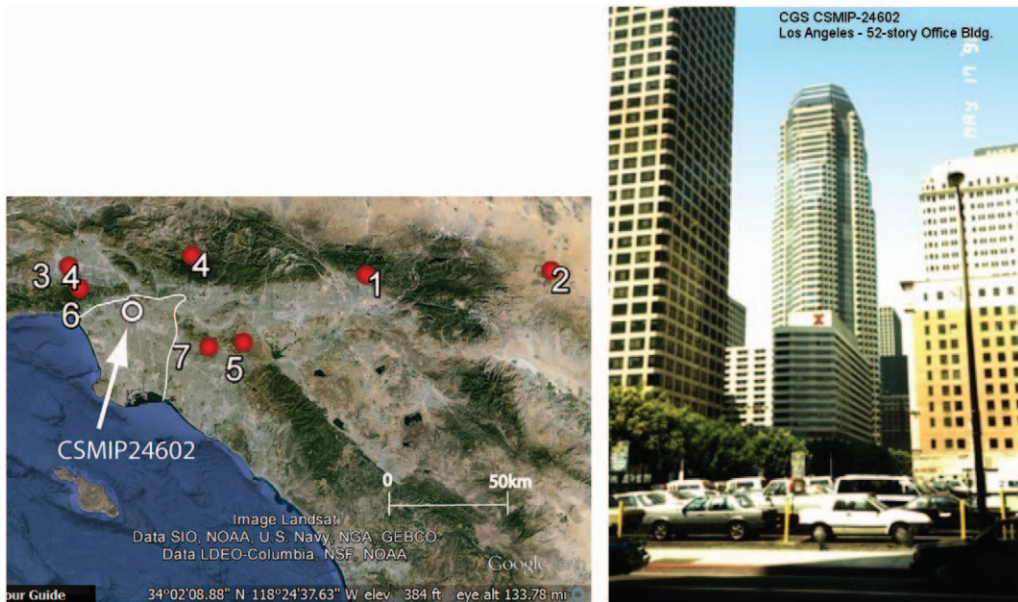


Figure 1. (a) Google Earth map modified to show relative locations of the building (CSMIP24602) and the epicenters of the events (Table 1) recorded. The building is founded in the Los Angeles Basin. All of the seven events shown in the map originated outside of the Los Angeles Basin. (b) CSMIP picture of the building [Latitude: 34.0507N, Longitude: 118.2595W, Elevation: 89 m.] (<http://www.strongmotioncenter.org>).

events that occurred at varying distances. However, when referring to a “near” or “far” earthquake, there is no clearly distinguished definition of “near” or “far.” A good rule of thumb to distinguish between a near and a far earthquake is a distance equivalent to the length of the fault considered (D. Boore, *pers. comm.*, 2015). By that rule, therefore, the event data used in the paper are considered to be from far distant earthquakes relative to the building in downtown Los Angeles. These seven events were recorded by the building seismic instrumentation array installed in 1990 by the California Strong Motion Instrumentation Program (CSMIP) of California Geological Survey (CGS; www.strongmotioncenter.org). However, there are no free-field stations in close proximity to the building to facilitate comparison of free-field recorded motions with those recorded in the basement of the building. The closest free-field station (CGS24289) is approximately 850 m away. Nonetheless, the seven earthquakes recorded by the building array display excitation of the building at varying amplitudes of accelerations and displacements at the basement and the roof, as well as other instrumented floors.

The building was studied extensively by Ventura and Ding (2000) for events recorded prior to 2000. To the best of our knowledge, besides this study, there is no other relevant and detailed study related to seismic responses of the building. In addition to finite element method (FEM) analyses, Ventura and Ding (2000) obtained dynamic characteristics using earthquake response records during the 1994 M_w 6.7 Northridge and the 1991 M_w 5.6

Sierra Madre earthquakes and compared the computed fundamental periods by using both FEM and recorded data with those computed during the original structural design process. Furthermore, the Ventura and Ding study also performed nonlinear analyses using earthquake ground acceleration data recorded elsewhere. Later in this paper, we take advantage of this information and compare our results with the Ventura and Ding study. Note that the present study also makes use of the data from the 1992 M_w 6.5 Big Bear, 1992 M_w 7.3 Landers, and three other earthquakes that occurred after 2000 (Figure 1 and Table 1). Both the Big Bear and Landers earthquakes occurred at epicentral distances greater than 100 km from this building. Thus the motions generated by these two earthquakes, as well the other earthquakes, passed into and reverberated within the Los Angeles Basin and impacted this building with long period motions of the basin. It is likely that other earthquakes at much closer epicentral distances from downtown Los Angeles (e.g., less than 25 km) could also generate basin motions to influence the building response.

Long-period responses of structural systems at large distances have been observed for many earthquakes, and in particular for tall buildings. One of the earliest observations in the United States was during the $M = 7.3$ Kern County earthquake of 7 July 1952, that shook many taller buildings in Los Angeles and vicinity, about 100–150 km away from the epicenter (http://earthquake.usgs.gov/earthquakes/states/events/1952_07_21.php; Hodgson 1964). The 28 March 1970, $M = 7.1$ Gediz earthquake in inland western Turkey damaged several buildings at a car-manufacturing factory in Bursa, 135 km northwest of the epicenter

Table 1. Recorded events in chronological order and particulars of records from CSMIP Station 24602 (event info from <http://www.stronmotioncenter.org/>, last accessed April 16, 2015) including largest peak accelerations, velocities and displacements at Ground Level (GrFl) [actual E-Level] and top instrumented (TopFl) floor [roof] of the building. Building coordinates are: 34.0507N, 118.2595W.

Event	Date and local time	Name of Event & Epicenter Coordinates	M_L M_w	Dist (km)	Largest Hor. Peak Acc (gals) (Gr Fl/Top Fl)	Largest Hor. Peak Vel (cm/s) (Gr Fl/Top Fl)	Largest Hor. Peak Disp(cm) (GrFl/TopFl)
1	199206280805	Big Bear Eq 92 34.20N, 116.83W	6.5	133	30/100	4.17/16.3	1.20/6.3
2	199206280457	Landers92 34.22N, 116.43W	7.3	169	50/170	8.70/49.8	9.81/40.8
3	199401170430	Northridge 34.21N, 118.54W	6.7	31	150/410	8.41/40.3	3.10/21.9
4	199106280743	Sierra Madre 34.26N, 118.00W	5.8	33	90/230	5.07/13.9	0.98/4.3
5	200807291142	ChinoHills 33.95N, 117.77W	5.4	47	63/263	5.20/19.1	0.86/2.9
6	201403170625	Encino 34.13N, 118.49W	4.4	22	14/19	0.29/1.0	0.06/0.3
7	201403282109	LaHabra 33.93N, 117.92W	5.1	34	16/48	1.35/6.5	0.45/1.9

(Tezcan and Ipek 1973). During the 19 September 1985, Michoacan, Mexico, $M = 8.0$ earthquake, at approximately 400 km from the coastal epicenter, Mexico City suffered more destruction and fatalities than the epicentral area due to amplification and resonance (mostly around 2 s) of the lakebed areas of Mexico City (Anderson et al. 1986, Çelebi et al. 1987). To the best of our knowledge, however, there are no publicly available records of the responses of tall structures from these cited past earthquakes.

According to Rahmani and Todorovska (2014a, 2014b), there are records obtained by CSMIP from only a few instrumented tall buildings in Los Angeles during several earthquakes between 1992 and 2010, with the largest magnitude ($M_w 7.3$) 1992 Landers earthquake. Recently, Rahmani and Todorovska (2014a) studied responses of a 54-story tall building (CSMIP 24629) in close proximity to the building (CSMIP 24602) that is subject of our study. However, their study did not extend to possible basin effects on the responses of that building. As will be shown later, not surprisingly, both tall buildings have very similar basin depth–shear wave velocity (V_S) profiles. Therefore, it is very likely that in that part of downtown area, many other existing tall buildings and new ones under construction (e.g., the 73-story core shear wall Wilshire Grand Building with outrigger frames under construction in downtown Los Angeles) or being designed will also be subjected to basin effects similar to the building in our study. Thus, studies of records from instrumented tall buildings built on deep basins will be useful for assessment of the behavior and performances of other tall buildings on similar geological environments. That is one reason why this study makes use of such response records from the 52-story tall building (CSMIP 24602) in Los Angeles Basin.

It can be stated that, worldwide, very few percentage (e.g., $\ll 1\%$) of tall buildings¹ are instrumented. However, on the positive side, significant response records were obtained from the few instrumented tall buildings during the 2011 Tohoku earthquake ($M_w 9.0$). As an example, an earlier study (Çelebi et al. 2012, 2014) revealed that a 55-story building in Osaka, Japan, 770 km away from the epicenter of the main shock of the 2011 Tohoku earthquake, resonated vigorously for about 140 s of the 1,000 s-long record with an input peak acceleration of 3% of g , or 0.03 g (amplified due to site conditions). In that study, it was shown that in addition to the effects of long-period motions, a combination of site resonance (e.g., structural fundamental frequency ~ 0.15 Hz and site frequency ~ 0.13 – 0.17 Hz) and low structural damping (~ 1 – 2%) caused the building to experience significant prolonged responses for 1,000 s and roof displacement with a peak value of ~ 130 cm. This amplitude of peak roof displacement translates into an average drift ratio of $\sim 0.5\%$ which, in Japanese practice, is the starting point of damage (Kubo et al. 2011). Other studies of recorded responses of tall buildings in Tokyo during the 2011 Tohoku earthquake show similar trends of low structural damping ($< 3\%$), permanent shifts of fundamental periods and indications that the responses are affected by basin effects (Çelebi et al. 2016a, 2016b). Therefore, studying possible basin effects and extraction of dynamic characteristics (e.g., frequencies and damping) and behavior of the subject building in downtown Los Angeles constitutes an important motivation for this paper.

¹ In this paper, although we study a 52-story building, normally, buildings > 10 stories are considered to be tall.

In addition, during several earthquakes originating in Iran, several instrumented tall buildings in some of the Gulf States (e.g., Dubai and Abu Dhabi) at distances as large as 800 km from the epicenters were shaken strongly and valuable records were obtained. For example, Abdulrazaq (2012) reports on records obtained during the 10 July 2010 earthquake in Iran from the seismic array installed in Bhuj Khalifa, the current tallest building of the world, in Dubai. Similarly, seven tall buildings in Abu Dhabi recorded responses during earthquakes in Iran (E. Safak, *pers. comm.*, 2015). However, most of the significant majority of recorded data are not made public. Thus, available data sets from instrumented tall buildings in the United States or elsewhere (e.g., Japan) are even more important for studying and understanding how the behavior and performances of long-period structures (e.g., tall buildings, long-span bridges) are characterized by predominantly long-period responses during medium-to-large events originating at far distances.

Therefore, the objectives of this study are to: (1) take advantage of data already acquired from one of the few instrumented tall buildings in Los Angeles; (2) deliberate on possible effects due to geological setting of the building (e.g., basin effects) and thus draw attention to impact of basin effects for tall buildings built in a basin; (3) to extract significant and meaningful results from the data, including dynamic characteristics, information related to behavior (e.g., beating effects), and, if possible and mostly for large responses, the performance of the building (e.g., large drift ratios, if any); and (4) draw conclusions from the results of analyses of the tall building studied herein.

In this paper, we used spectral analyses techniques as described in Bendat and Piersol (1980) and coded in Matlab (Mathworks 2012). We also use system identification techniques (e.g., Ljung 1977) to extract mode shapes and associated frequencies and damping. Finite element analyses of the building are outside the scope of the paper.

THE BUILDING AND SEISMIC INSTRUMENTATION

Schematics with dimensions and locations of accelerometers distributed throughout the building are shown in Figure 2. The number of stories above/below ground are 52/5. The height of the building above the ground is 218.1 m. Base dimensions are 83.5 m \times 80.2 m (274 ft \times 263 ft). The core area of the building is 21.3 m \times 17.4 m (70 ft \times 57 ft) and extends from the 1st sub-basement all the way to the roof. All floors of the tower structure as well as those at the imprint of the tower at the basement (Level E) are symmetrical in both directions (e.g., from 1st floor to 45th floor, the in-plan overall dimensions are 47.5 m \times 47.5 m (156 ft \times 156 ft); then reducing at the roof to basically the core area. The vertical load carrying system comprise 7.6–17.8 cm (3–7 in.) concrete slabs on steel deck supported by steel frames. The main foundation system is concrete spread footings 2.7–3.3 m (9–11 ft) thick (from <http://www.stromotioncenter.org/>).

Twenty accelerometers installed by CSMIP are distributed throughout the building to acquire mainly translational and torsional responses. However, average drift ratios can be computed using displacements computed from double-integrated accelerations from any two instrumented floors. Seven instrumented floors have two parallel accelerometers that allow computation of torsional behavior of the building. There is only a single vertical accelerometer at the center of the core area (Figure 2). This prohibits direct computation of rocking motions of the foundation and the superstructure.

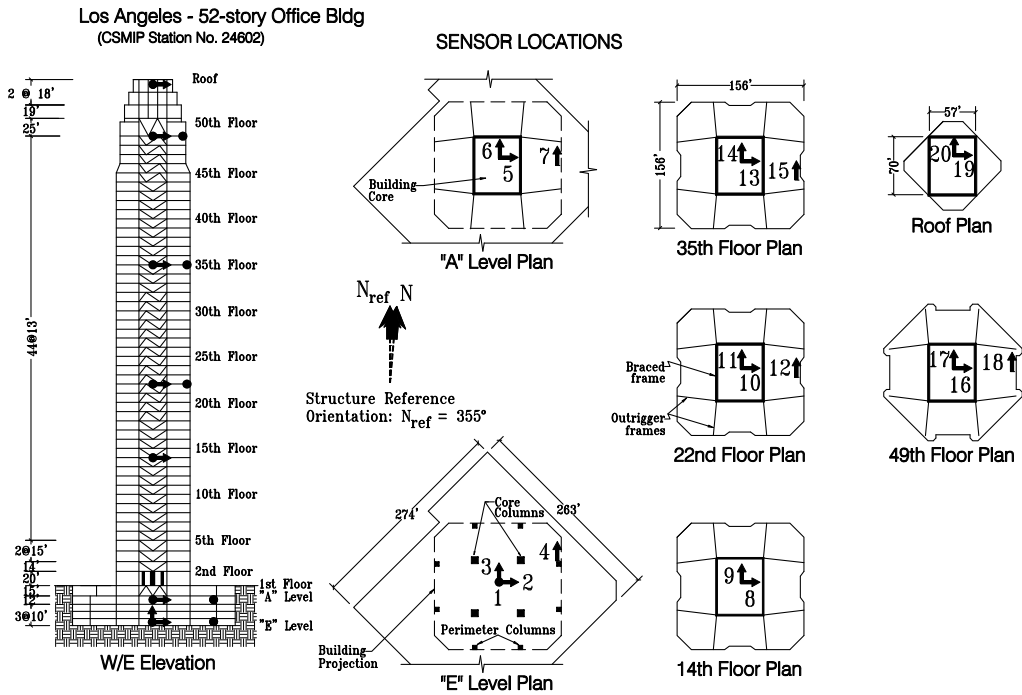


Figure 2. Schematic of vertical section and plan views as well as accelerometer deployment locations (from <http://www.strosmotioncenter.org/>).

Table 1 shows seven events with recorded responses of the building and peak values of motions at E level (Figure 2) and top instrumented floor (roof).

SITE ISSUES

The site geology of the building is defined as alluvium over sedimentary rock (www.strosmotioncenter.org). Detailed borehole data at the top 100–200 m is not available. Nonetheless, in order to compute site transfer functions for low frequency bandwidth (<1 Hz), we used the Southern California Earthquake Center (SCEC) seismic velocity model (SCEC CVM-H version 5.3) for Los Angeles Basin derived from sonic logs and industry reflection data (Süss and Shaw 2003). Figure 3a shows the depth–shear wave velocity (V_S) profile representative of the sites of the two tall buildings [CSMIP stations 24602 (this study) and, as mentioned before, in close proximity to another tall building instrumented, CSMIP station 24629]. The two tall buildings are ~ 350 m apart and their V_S -depth profiles are similar and, most likely, also similar to profiles of sites of other tall buildings in the area that are (or not) instrumented. The second site is included primarily to draw attention to the basin effect so that future studies of existing and future long-period structures in that area can make use of this similarity. Computed transfer function using the approximated V_S -depth step-profile C is shown in Figure 3b and demonstrates and infers significant amplification of motions at particularly low frequencies <0.5 Hz. Minor changes in approximated

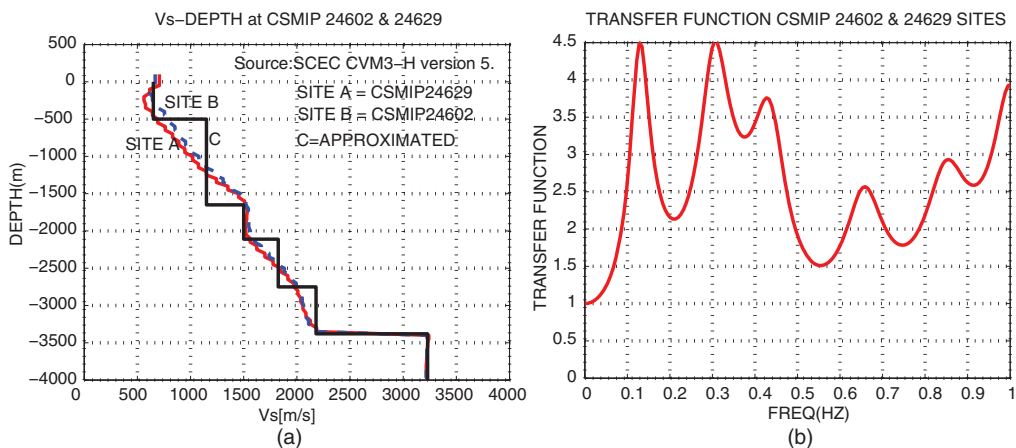


Figure 3. (a) V_S -depth profile [from SCEC CVM-H version 5.3] for downtown Los Angeles [Site A (red line) and Site B (dashed black line)] represent sites of tall buildings with CSMIP station numbers 24602 (this study) and 24629. The profile C (step-line) represents approximated profile for both building sites. Alternate variations of approximations of step-profile should not alter the results significantly. Both tall buildings are in close proximity with each other (~ 350 m apart), and thus the results are representative of other tall buildings in the vicinity. (b) Transfer function is computed using approximated step profile C for both sites.

step-profile do not affect the inference that the fundamental site frequency is low (~ 0.12 – 0.13 Hz). In computing the transfer function, software developed by Mueller (*pers. comm.*, 2005) based on Haskell's shear wave propagation method is used (Haskell 1953, 1960). In this method, the transfer function is computed using linear propagation of vertically incident SH waves. Input data comprises those related to the layered media (number of layers, depth of each layer, corresponding V_S , damping, and density), desired depth of computation of transfer function, sampling frequency, half-space substratum shear-wave velocity, and density. Damping (ξ) in the software is provided as Q , a term used by geophysicists, and is related to critical damping ratio used by engineers by $\xi = 1/(2Q)$. Q values used in calculating the transfer functions are between 25 and 60 for shear-wave velocities between 200 m/s and 600 m/s. V_S and Q are approximately interpolated to vary linearly within these bounds. To reiterate therefore, the resulting illustrative transfer function shows significant low frequency peaks for <0.5 Hz. For example, the first peak at ~ 0.12 – 0.13 Hz, if coincident with the fundamental frequencies of tall buildings at close frequencies could result in resonating responses.

ANALYSES OF DATA

EQUI-SCALED TIME HISTORIES FOR SEVEN EARTHQUAKES, AMPLITUDE SPECTRA, AND TRANSFER FUNCTIONS

Figure 4 shows the acceleration time histories for the 7 events identified in Table 1. Event records have different length. Figure 5 shows a similar plot for displacements. It is clear from

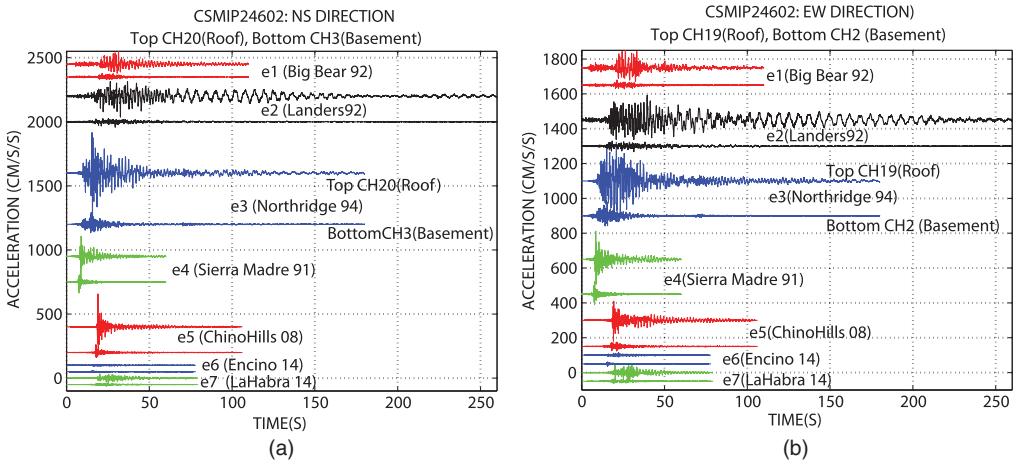


Figure 4. Equi-scaled accelerations at basement and roof of the building for seven events: (a) NS direction, (b) EW direction.

Figure 4 and Table 1 that the Landers earthquake (M_w 7.3; Event 2) that occurred farthest (at 169 km epicentral distance) from the building has the largest velocity and displacement responses at the basement and the roof but not the largest accelerations. On the other hand, the Northridge earthquake (M_w 6.7; Event 3) that occurred at 31 km epicentral distance generated the largest accelerations at the basement and the roof. Most likely, long-period motions of large magnitude Landers event (M_w 7.3) that originated at the farthest distance coupled with basin effects (Figure 3) caused the larger displacements at the basement and the

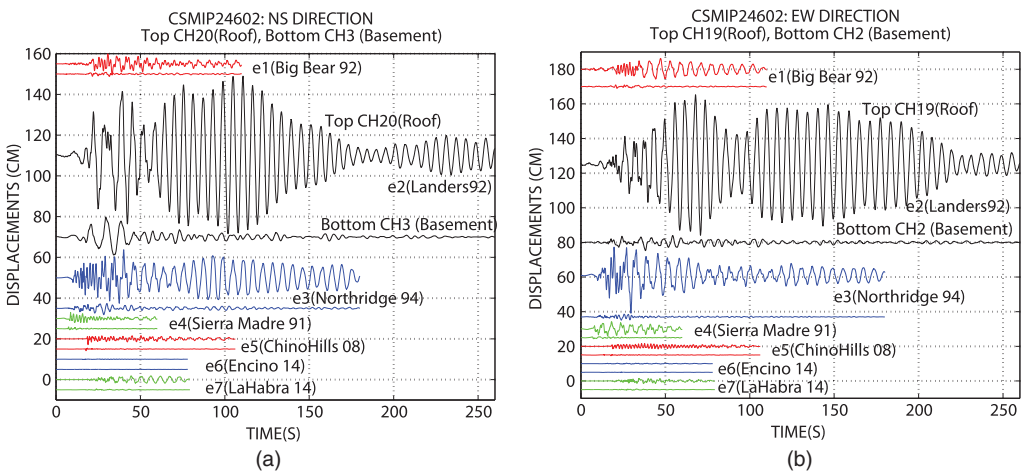


Figure 5. Equi-scaled displacements at basement and roof of the building for seven events: (a) NS direction, (b) EW direction.

roof of the building (Figure 5). To substantiate this, we computed acceleration and displacement response spectra from both Landers and Northridge accelerations recorded at the basement (E-level; see Figure 3) and roof of the building (Figure 6). The figure shows that at close to 6 s (or ~ 0.17 Hz), both the roof spectral acceleration and spectral displacements for Landers are approximately three times that for Northridge. Similarly, the spectral displacements at ~ 6 s at the base (E-Level) are larger for Landers compared with Northridge (by a factor of 2).

As noted in Table 1, the largest displacement at the roof level is ~ 41 cm, which, when divided by the height above first floor (218 m), translates into an average drift ratio of $\sim 0.19\%$. Therefore, at this level of average drift ratios, no structural damage is expected.

Figure 7 shows for 0–5 Hz and 0–2 Hz bandwidths normalized amplitude spectra of NS, EW and torsional accelerations at the roof. Figure 8 shows for 0–5 Hz and 0–2 Hz bandwidths transfer functions of amplitude spectra of NS, EW, and torsional accelerations at the roof with respect to the basement. From both Figures 7 and 8, we can claim that by these spectral analyses, at least the first 3 modes in each direction are clearly identifiable (NS: 0.17, 0.57 and 1.05 Hz; EW: 0.17, 0.55, 1.08 Hz; torsional: 0.17–0.18, 0.55, and 1.08 Hz). These frequencies identified simply by peak-picking show consistency with small variations of about 0.1 Hz mostly for the second and third modes. Furthermore, translational and torsional modes are coupled at these frequencies. The fourth mode exhibits greater variation. This may be real or it may be due to computations and smoothing of the spectra.

In addition, the fact that for both amplitude spectra and ratios of amplitude spectra for the lower modes are very similar indicates the frequencies computed from structural response data are not affected by soil-structure interaction. In any case, because there is only one vertical accelerometer deployed right at the center of the imprint of the tower, direct computation of rocking rotation of basement around a horizontal axis is not possible.

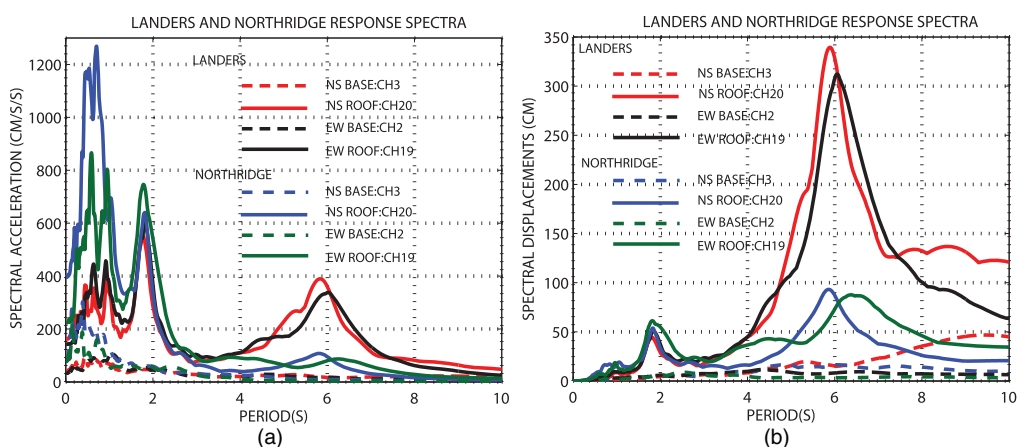


Figure 6. Comparison of Landers and Northridge (a) acceleration and (b) displacement response spectra computed from accelerations recorded at base (E-Level) and roof of the building.

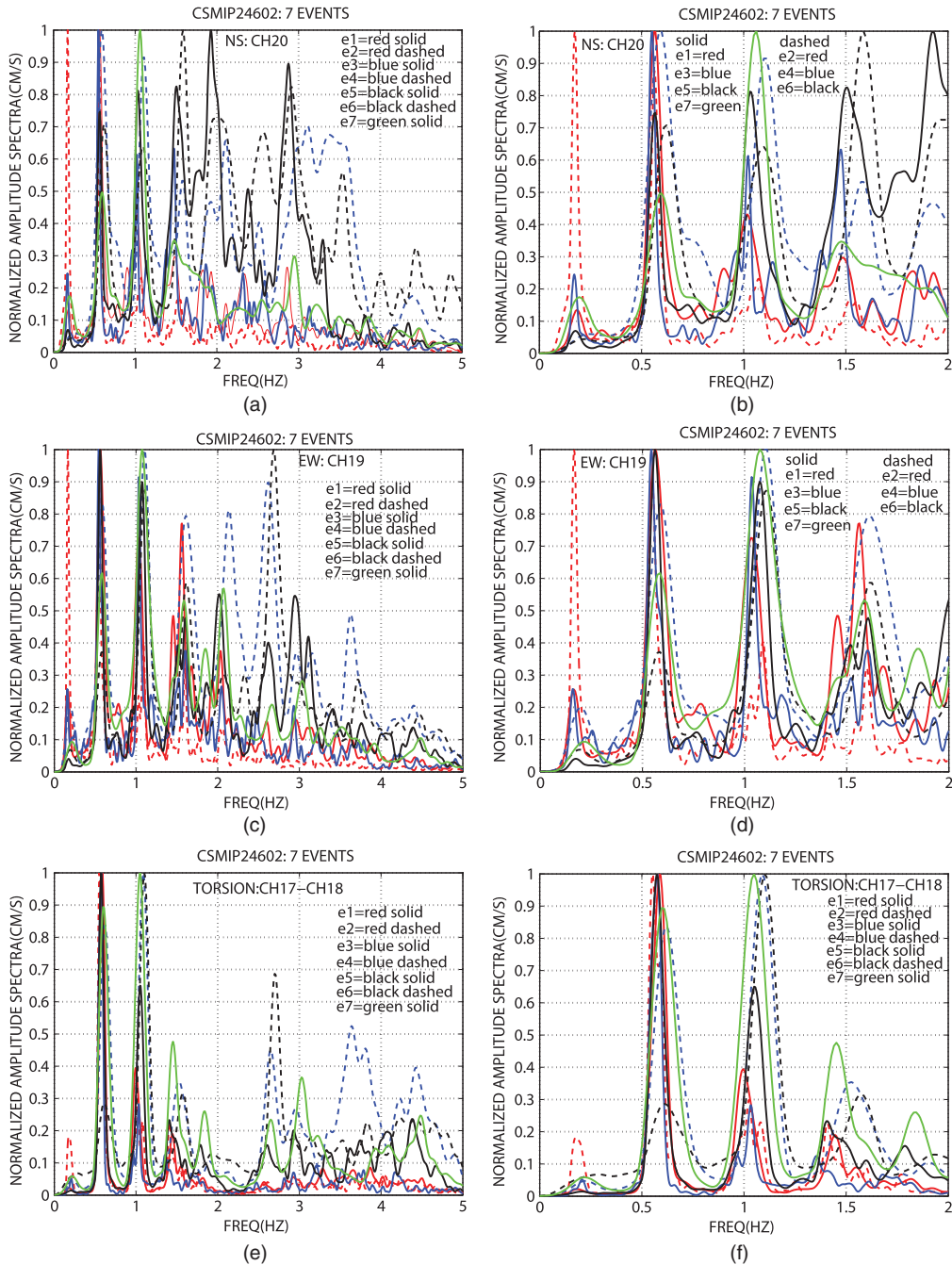


Figure 7. Normalized amplitude spectra of accelerations at the roof for 0–5 Hz and 0–2 Hz bandwidth respectively in (a) and (b) NS direction (CH20), (c) and (d) EW direction (CH19) and (e) and (f) torsion (CH17–Ch18).

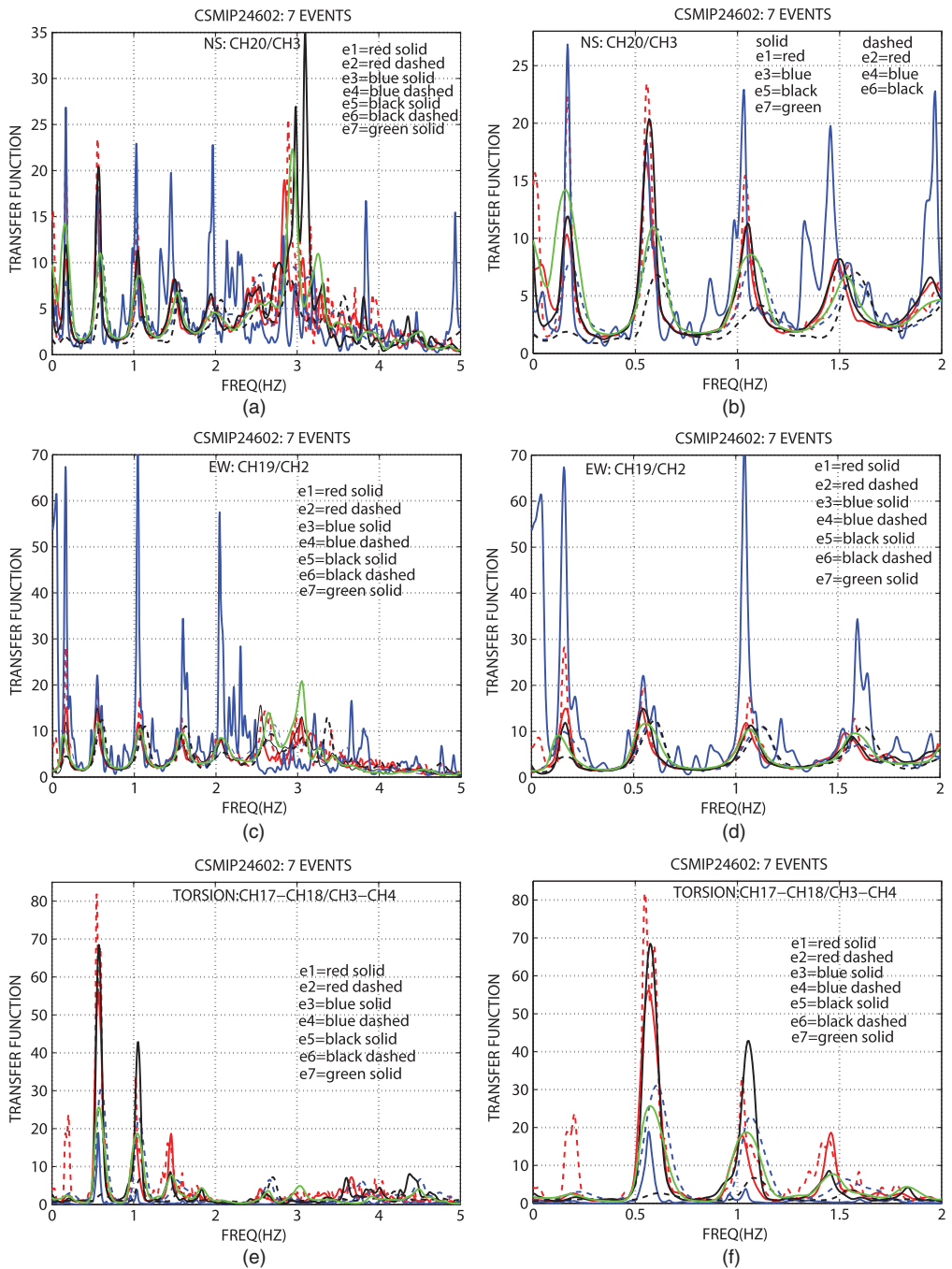


Figure 8. Transfer functions computed from amplitude spectra of accelerations at the roof and basement for 0–5 Hz and 0–2 Hz bandwidth respectively in (a) and (b) NS direction (CH20/CH3), (c) and (d) EW direction (CH19/CH2) and (e) and (f) torsion [(CH17–Ch18)/(CH3–CH4)].

One consistency is the closeness of translational (both NS and EW) and torsional fundamental frequencies, inferring coupling of the translational-torsional responses, potentially causing beating effects as explained later in the paper.

COHERENCY AND PHASE

To further confirm the modal frequencies, we performed coherency and phase analyses of roof and 14th-floor responses of the building in the NS and EW directions for Event 2 (Landers; Figure 9a) and for Event 3 (Northridge; Figure 9b). Clearly coherencies are ~ 1 for the first 4 modes and phases (for the first and third modes are 0° and in phase and for the second and fourth modes are 180° and out of phase). Therefore, the frequencies identified by peak picking are reliable.

SYSTEM IDENTIFICATION METHODS AND APPLICATIONS

Spectral analyses methods are powerful in identifying modal frequencies from amplitude spectra, spectral ratios and cross-spectra applications. Usually, peak picking approach is used to extract the modal frequencies from spectra or spectral ratios. However, these particular applications are not generally useful in estimating modal critical damping percentages (ξ) and mode shapes, although damping percentages (ξ) can sometimes be estimated by half bandwidth method using the shape of the spectra.

Therefore, in order to obtain critical damping percentages and mode shapes, in addition to modal frequencies, we use system identification methods to compute and/or validate dominant frequencies and compare them with those determined by spectral analyses. Two of the

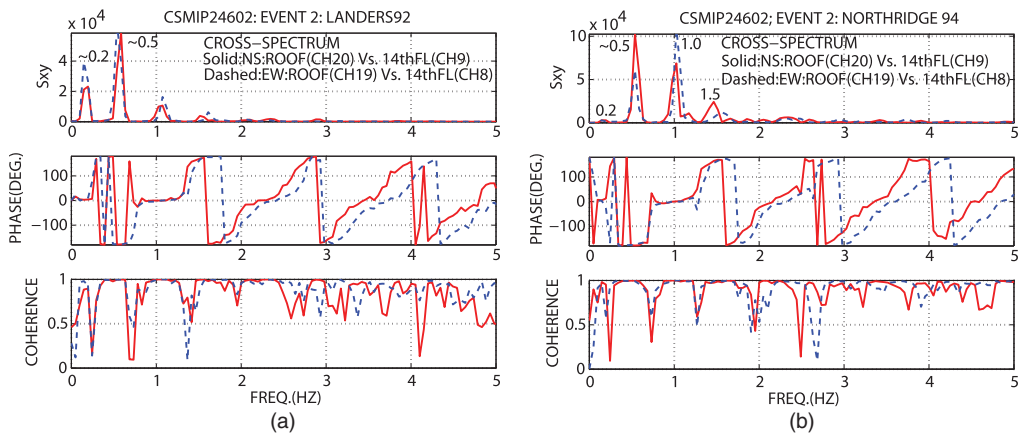


Figure 9. Cross spectra, phase angles and coherencies of NS and EW acceleration at the roof (a) versus 14th floor for Event 2 (Landers) and (b) Event 3 (Northridge) earthquakes show excellent coherency and correct phase angles for the first four modes (0° and in phase for the first and third modes and 180° and out of phase for the second and fourth modes). The frequencies shown are rounded numbers. More accurate numbers are identified from peak picking of transfer functions or system identification that yields mode shapes and modal damping.

more widely used methods of system identification, also applied in this study, differ in requirement of input/output data. Thus, the two system identification methods used herein provide an opportunity to compare the computed frequencies by the two methods as well. The third method is used to demonstrate utilization of seismic interferometry method to extract modal frequencies and damping within a frequency band.

A method known as N4SID (Numerical Algorithms for Subspace State Space System Identification) is the first system identification method used herein (Overschee and DeMoor 94). In this method, measured data from the building is used to estimate a predefined number of order of state-space model using the subspace method as coded within Matlab (Mathworks 2013). Further details of background of this method are not repeated herein as they are provided in many other publications including Ljung (1999), Van Overschee and De Moor (1996), and Juang (1994). Essentially all data including those at basement or ground floor of a building are used as output.

The second method is another state space system identification algorithm known as the multivariable output error state space (MOESP) to derive the state space models that represent the dynamics of the building during earthquakes. The dynamic characteristics of the building [modal frequencies, damping ratios, and the associated mode shapes] are extracted from the state space models. The MOESP algorithm requires both excitation and response measurements. Data from the basement floor are used as input and remaining data from other floors are used as output. In this algorithm, the measured data are stored in block Hankel matrices first. Then, the QR matrix decomposition of the data matrices consisting of the block Hankel matrices is computed to estimate the orthogonal projection of future output onto the past input and past output. The singular value decomposition of the orthogonal projection is used to determine the system order, the extended observability matrix and later, the system matrices. Further details of the MOESP can be found in Verhaegen (1994).

Both system identification methods N4SID and MOESP are two numerical algorithms for finding a representative linear state space description of a dynamical system from input (excitation) and output (response) measurements. They differ in the way the observability matrix is estimated, and how it is used for finding system matrices. In N4SID algorithm, the *oblique* projection of the row space of the future output along the row space of the future input onto the row space of the past input and past output is used to compress data, determine the system order, and estimate extended observability matrix. On the other hand, in MOESP algorithm, the *orthogonal* projection of the row space of the future output onto the row space of the past input and past output is used to estimate the extended observability matrix. An excellent discussion about the similarities and differences between various state space system identification algorithms are provided by Viberg (1994) and Overschee and DeMoor (1994).

For earthquake engineering applications, these two algorithms work equally well in identifying dominant vibration frequencies and associated mode shapes and damping ratios. Despite, frequency domain technique that require a fairly longer data to obtain a smooth spectra or the frequency response function, these time domain algorithms work better for earthquake data which are typically 1–2 minutes long. These algorithms provide excellent results in cases where vibration modes of a structure are very close, for instance, the building in this study.

The third method, seismic interferometry, is an approach to analyze the response of the building using a wave propagation model. The additional advantage of the seismic interferometry is that an average shear wave velocity through the building can be estimated from wave travel time. This method is not intended to identify modal parameters of the building but confirm the previous results in part generated by the first two (N4SID and MOESP) methods.

APPLICATION OF THE N4SID METHOD

Results obtained by N4SID system identification method are provided in Figures 10a and 10b for Landers and Northridge earthquakes, respectively. The figures show the first three identified mode shapes, modal frequencies and damping ratios for each of the NS bending, EW bending and torsional modes. The frequencies compare well with those from spectral analyses using peak picking method. Both the frequencies and critical damping percentages are inserted into the figures.

APPLICATION OF THE MOESP METHOD

The horizontal response of the building measured at seven levels in the reference EW and NS directions is used to identify the state space models (see sensor layout in Figure 2). The two sensor recordings 2 and 3 at level E are used as the excitation and 16 sensor recordings from 5 to 20 at six different levels are used as the response. The MOESP algorithm is applied to the 1992 Landers and the 1994 Northridge earthquakes to identify the dominant modes of the building that significantly participate in the total response. The analysis suggests that the first three bending modes in each of the EW and NS directions and the first three torsional modes dominate the response. The extracted mode shapes of the building are shown in Figure 11a and 11b for Landers and Northridge earthquakes, respectively. As before, the

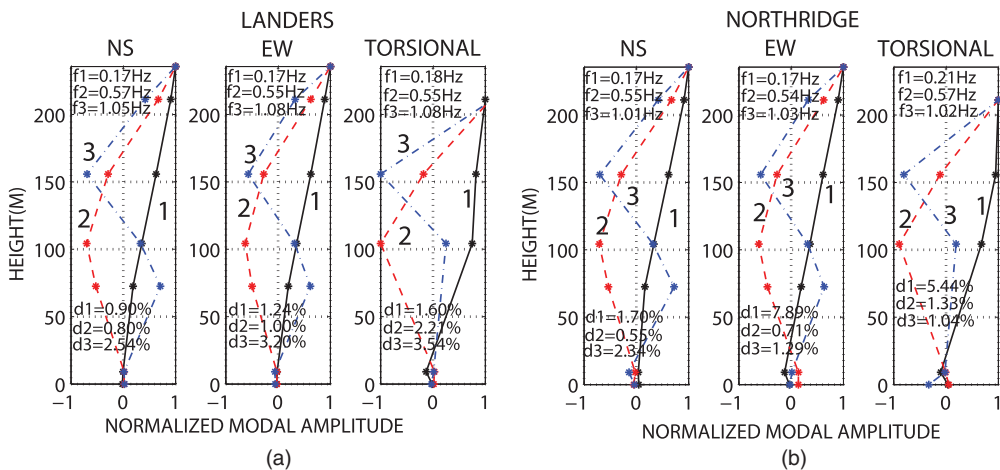


Figure 10. Using the N4SID method, three for each of NS bending, EW bending and torsion modes using the (a) Landers and (b) Northridge earthquake accelerations are shown. Identified frequencies and critical damping percentages (abbreviated as d) are also shown. Mode numbers are indicated.

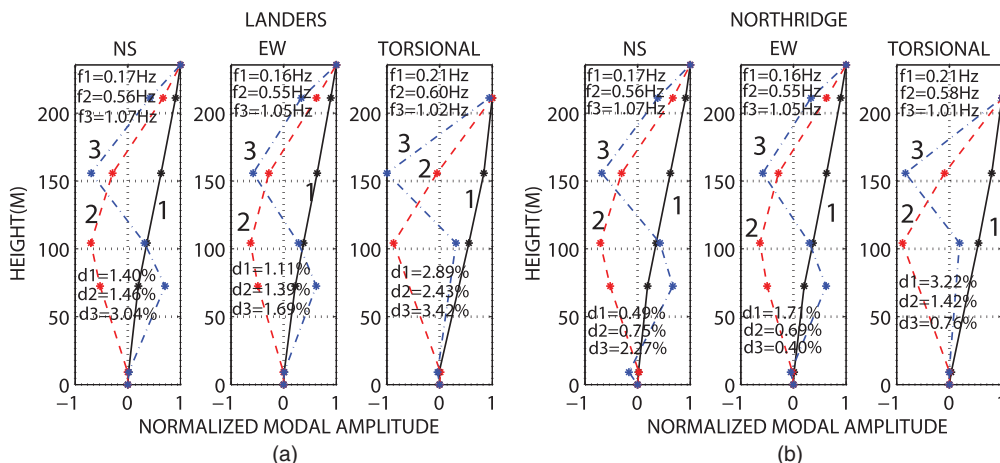


Figure 11. Using the MOESP method, the first three bending modes of the building identified from the (a) 1992 Landers Earthquake and (b) 1994 Northridge Earthquakes are shown. Identified frequencies and critical damping percentages (abbreviated as d) are also shown. Mode numbers are indicated. The mode shapes are extended to zero “height” only for continuity of the plots.

associated frequencies and damping ratios of the first three bending modes in both directions and the first three torsional modes are included in each frame of the figures.

The observed frequencies of the buildings during different earthquakes may vary depending on earthquake intensity, distance, and other structural factors (Ulusoy et al. 2011). However, for these two particular earthquake records, the frequencies and damping ratios of the building identified are quite consistent. The mode shapes are also compared to measure the consistency of the modes using modal assurance criterion (MAC; Allemang 2003). The MAC values for the mode shapes identified are almost equal to 1 indicating that the two sets of mode shapes, for all practical purposes, are almost identical.

APPLICATION OF THE SEISMIC INTERFEROMETRY METHOD

To determine shear-wave travel time, shear-wave velocity and attenuation of traveling waves inside a building and damping, deconvolution based seismic interferometry method is used (Snieder and Safak 2006, Nakata and Snieder 2014). The observed wavefields recorded at each instrumented floor are deconvolved with wavefields at a selected floor. Response of the building extracted by deconvolution depends on which instrumented floor we choose for deconvolution (Nakata et al. 2013). In this study, the wavefields of the horizontal records at each instrumented floor of the building for the Landers earthquake are deconvolved with those records from the roof. When we choose the basement for the deconvolution, we obtain the transfer function shown in Figure 8. Assuming that there is no torsional and only vertical wave propagation inside the building, the deconvolved wavefields represent the upgoing and downgoing wavefields in the negative and positive times, respectively (Figure 12). Since horizontal components of recorded motions are used and vertical propagation is assumed, the extracted waves are interpreted as shear waves. As a result of the deconvolution, the

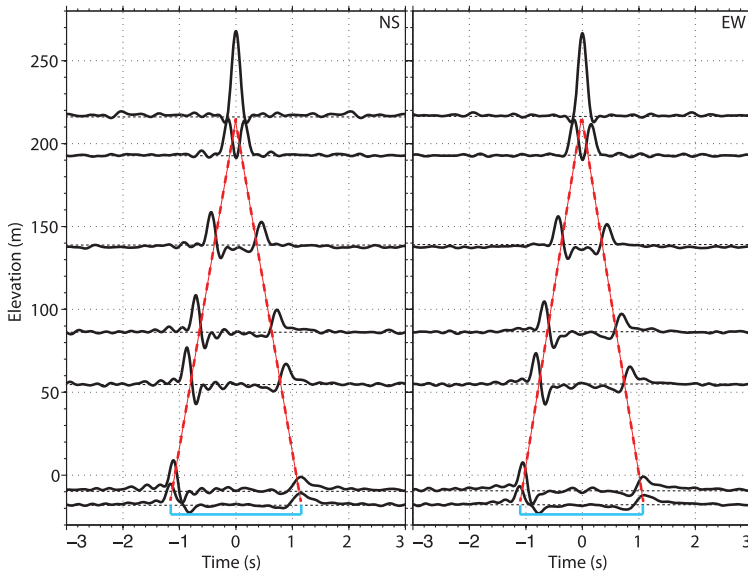


Figure 12. Waveforms of the Landers earthquakes at each instrumented floor after deconvolution with the record at the roof in the EW and NS components. A high-cut filter is applied at 4.0 Hz to include multiple modes to extract reliable traveling waves. The red lines indicate the travel times of the deconvolved waveforms. The blue time interval is the two-way travel time of the shear waves at the base.

wavefields at the roof become a band-limited delta function. Thus, we obtain an impulse response of the building. This virtual impulse source is at the roof (Nakata et al. 2013).

The dashed red lines in Figure 12 show the travel times of extracted upward and downward travelling waves. The blue lines indicate the two-way travel time of the deconvolved wavefields at the base. Hence, the velocity of the traveling waves is estimated by dividing distance traveled by travel time. Due to the shape of the building, we expect that we satisfy the assumption of the vertical wave propagation. The waveforms in the EW and NS components are almost identical, which indicates that the stiffness of the building in the NS and EW directions are almost identical. Following Snieder and Safak (2006), we estimate the shear-wave velocities and the frequency-independent Q values of the building from the deconvolved wavefields in Figure 12. As explained earlier, seismologists use Q values and engineers use critical damping percentage (ξ) [related to Q by $\xi = 1/(2Q)$]. It is noted that this is a frequency-independent Q . This analysis mixes information of all modes because the impulse response contains the response of all frequencies.

First, we measure the travel time of the maximum amplitudes in the negative and positive times at each instrumented floor in Figure 12. These times represent the arrival times of the deconvolved wavefields, and we can convert the arrival times to shear-wave velocities because we know the distance of propagation. Figure 13a shows the arrival times as a function of distance. Similar to Snieder and Safak (2006), we consider the traveling distance in the

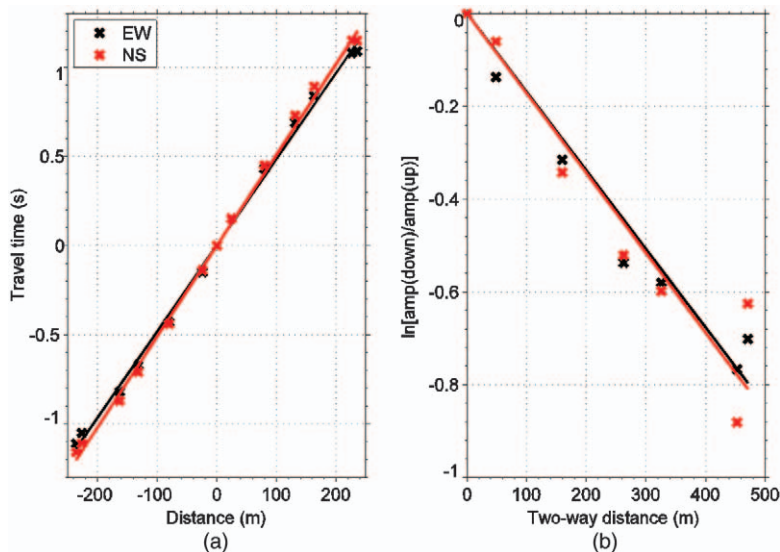


Figure 13. (a) Measured arrival times of the upgoing and downgoing wavefields at instrumented each floor in Figure 3. In each component, 13 crosses are plotted that correspond to arrival times of upgoing and downgoing waves at each floor. Note that the arrival time at the roof is fixed at time 0 s. The negative distances and travel times represent the upgoing wavefields, and the positive values the downgoing wavefields. The arrival time of the wavefields at the roof is at the origin. The solid lines indicate the travel times of the velocities estimated from the measured arrival times with least squares fitting. (b) Natural logarithm of the ratio of maximum amplitudes of the upgoing and downgoing wavefields in Figure 12. The two-way distance is the traveling distance of the deconvolved waves, and the two-way distance of the wavefields at the roof is at the origin. The least squares fitting lines are indicated with solid lines.

negative time is negative to satisfy the causality. When we assume a constant wave velocity in the entire building, we can estimate the velocity with least squares fitting of the measured arrival times at each component. For the fitting, we constrain the straight line to pass distance 0 m at time 0 s because this is in a definition of deconvolution interferometry. From the lines in Figure 13a, the wave velocities in the NS and EW components are 195.8 ± 0.9 m/s and 206.6 ± 1.0 m/s, respectively. The velocity is estimated by least-squares fitting for the arrival travel times of the waves at each instrumented floor, and the error range shows one standard deviation of the measurements. The slightly faster velocities in the EW component can be attributed to the shape or minor difference in stiffness of the building core.

To estimate Q , the amplitudes at the arrival time and compute the ratio of the amplitudes in the negative (upward) and positive (downward) travelling times are measured (Figure 13). As Snieder and Safak (2006) showed, this ratio is proportional to the attenuation between each floor and the roof of the building. When we consider one-dimensional (1-D) wave propagation, the amplitude decays with distance as $\exp(-\pi f z / Q v)$, where f is the frequency, v is the velocity of the wave, and z is the distance of propagation. From the slopes in Figure 13b and the velocities estimated above, Q 's in the NS and EW components are 18.7 ± 1.2

and 18.0 ± 0.9 . We use 2.0 Hz, which is the average or central frequency of the deconvolved wavefields, to estimate Q .

As a result of deconvolution analysis, velocities (195.8 m/s and 206.6 m/s) and Q (18.7 and 18.0) in both NS and EW components respectively are identified (e.g., approximately $\xi = 1/(2 \times 18) \sim 2.8\%$). These parameters represent the dynamic structural characteristics of the building. In the ideal case, the velocity can be linearly related to the frequency of the fundamental mode ($v = 4 * H * f$), where H is the height of the building (e.g., $f = v/4H \sim (200 \text{ m/s})/(4 \times 270 \text{ m}) \sim 0.185 \text{ Hz}$, very close to the fundamental frequency ($\sim 0.17 \text{ Hz}$) identified by other methods earlier in the paper. Because of the deconvolution, the waveform at the roof is a band limited delta function (Figure 12); therefore, the deconvolved waveforms and estimated parameters are related to an impulse response of the building.

COMPARATIVE RESULTS

In Table 2, we summarized our results for the first 3 modal frequencies and damping corresponding to Landers and Northridge earthquakes, the largest responses of all seven earthquakes. We compared these results with those from the only existing previous study of Ventura and Ding (2000). There is good match of the frequencies between the two studies. Damping was not reported in the Ventura and Ding (2000) study.

It is noted that in our study, for the Northridge earthquake, the damping for the first EW and torsional modes are considerably higher than those computed for the NS component and also for those computed for the Landers earthquake.

Table 2. Summary of frequencies (and periods) identified in this study and comparison with the studies of Ventura and Ding. Range of f/T numbers in parenthesis show values identified by Ventura and Ding (2000). This study includes damping (ξ).

	This Study (Measured)				From Ventura and Ding (2000)		
	f/T (Hz/s)		ξ (%)		f (Hz)/ T (s)		
	L	N	L	N	Design Value (**)	Measured (S_M and N results)	Analytical (N only)
NS(1)	0.17/5.88	0.17/5.88	0.90	1.70	0.15/6.56	0.17/(5.75–5.85)	0.18/5.61
EW(1)	0.17/5.88	0.17/5.88	1.24	7.89	0.15/6.23	(0.17–0.18)/(5.47–6.06)	0.17/6.00
(*)T(1)	0.18/5.56	0.22/4.55	1.60	5.44	0.16/6.36	(0.21–0.22)/(4.55–4.82)	0.21/4.75
NS(2)	0.57/1.75	0.55/1.82	0.80	0.55	0.47/2.11	(0.57/1.74)	0.57/1.77
EW(2)	0.55/1.82	0.54/1.85	1.00	0.71	0.48/2.08	(0.54–0.58)/(1.71–1.86)	0.54/1.85
T(2)	0.55/1.82	0.57/1.75	2.21	1.33	–	(0.55–0.62)/(1.62–1.82)	0.58/1.71
NS(3)	1.05/0.95	1.01/0.99	2.54	2.34	0.85/1.18	1.10/0.91	1.03/0.97
EW(3)	1.08/0.93	1.02/0.98	3.20	1.29	0.89/1.13	(1.04–1.09)/(0.92–0.96)	1.03/0.97
T(3)	1.08/0.93	1.02/0.98	3.54	1.04	–	(0.96–1.06)/(0.94–1.04)	0.96/1.04

Notes: (*) T = Torsional, (**) Design Values are adopted from Ventura and Ding (2000), S_M = Sierra Madre, N = Northridge, L = Landers earthquakes, ξ = damping

Table 3. Summary of identified frequencies (Hz) and critical damping percentages (ξ [%]) of the first three modes identified for the seven earthquakes. Landers and Northridge results (in italics) were reported in Table 2.

		Frequencies (Hz)			Damping ξ (%)		
		f_1	f_2	f_3	ξ_1	ξ_2	ξ_3
Big Bear	NS	0.18	0.56	1.01	0.99	0.88	0.42
1992	EW	0.16	0.56	1.03	1.35	1.20	1.46
06/28	Tor	–	0.60	1.00	–	.0184	0.76
<i>Landers</i>	<i>NS</i>	<i>0.17</i>	<i>0.57</i>	<i>1.05</i>	<i>0.90</i>	<i>0.80</i>	<i>2.54</i>
<i>1992</i>	<i>EW</i>	<i>0.17</i>	<i>0.55</i>	<i>1.08</i>	<i>1.24</i>	<i>1.00</i>	<i>3.20</i>
<i>06/28</i>	<i>Tor</i>	<i>0.18</i>	<i>0.55</i>	<i>1.08</i>	<i>1.60</i>	<i>2.21</i>	<i>3.54</i>
<i>Northridge</i>	<i>NS</i>	<i>0.17</i>	<i>0.55</i>	<i>1.01</i>	<i>1.70</i>	<i>0.55</i>	<i>2.34</i>
<i>1994</i>	<i>EW</i>	<i>0.17</i>	<i>0.54</i>	<i>1.03</i>	<i>7.89</i>	<i>0.71</i>	<i>1.29</i>
<i>01/17</i>	<i>Tor</i>	<i>0.21</i>	<i>0.57</i>	<i>1.02</i>	<i>5.44</i>	<i>1.33</i>	<i>1.04</i>
Sierra Madre	NS	0.18	0.57	1.08	2.74	2.52	1.09
1991	EW	0.18	0.57	1.09	3.20	1.34	1.00
06/28	Tor	–	0.60	1.07	–	0.86	0.36
Chino	NS	0.17	0.57	1.04	1.04	1.00	1.73
2008	EW	0.17	0.61	1.07	1.01	1.26	1.34
07/29	Tor	–	0.57	1.05	–	0.48	0.80
Encino	NS	–	0.60	1.08	–	1.24	1.93
2014	EW	0.18	0.57	1.09	.021	2.83	1.18
01/17	Tor	–	0.55	1.09	–	0.94	0.61
La Habra	NS	0.18	0.58	1.05	2.43	2.21	0.83
2014	EW	0.18	0.57	1.06	5.68	0.97	2.35
03/28	Tor	–	0.58	1.03	–	1.21	0.63

Dash (–) indicates it was not possible to extract the frequencies or damping for cases indicated. Tor = Torsional.

This prompted the computation of the frequencies and damping percentages for the first three modes of the remaining five earthquakes using N4SID system identification method previously described. We tabulated these characteristics for all seven earthquakes in Table 3.

We did not find reliable correlation of damping percentages between the shaking level of the seven earthquakes. However, the general trend of lower damping percentages is consistent.

BEATING EFFECTS

Beating effects, observed in several building response records in the past, occur when translational and torsional periods are close to one another and the structural system has low damping (Boroschek et al. 1990, 1991; Çelebi, M., 2004, 2006). Also, beating effects may explain one of the reasons for elongated durations of “replenished” shaking when repetitively stored potential energy during coupled translational and torsional deformations turns into repetitive vibrational energy. Thus periodic, repeating and resonating motions ensue. The beating becomes severe if the system is lightly damped. The beating effect period (T_b) is

computed using the relationship: $T_b = 2T_1T_t/(T_1 - T_t)$ given by Boroschek and Mahin (1991). In this relationship, T_1 and T_t are fundamental translational and torsional periods, respectively. A study of the responses of two tall buildings in Anchorage, AK, showed that beating effects occurred during several earthquakes due to identified closeness of the fundamental translational and torsional periods and low damping (Çelebi 2004, 2006).

In this study, we reiterate that translational and torsional fundamental frequencies are very close and/or coupled. Furthermore, very low damping percentages (0.9–1.24%) are identified for Landers (see Figure 9 and Table 2) and Northridge (in the NS direction ~1.7%). Visually and within the record length available, records of this building (Figure 5) from both Landers and Northridge earthquakes exhibit responses displaying beating effects. However, the displayed beating periods are not consistent – varying between 80–130 seconds for these two earthquakes. Whether beating responses occurred during Big Bear and Sierra Madre events cannot be confirmed due to short lengths of the actual records. However, in this study, to accurately quantify the period of a beating cycle (by the cited formula) is difficult since the translational and torsional frequencies are very close to one another or identical and coupled – which makes the computation using the formula meaningless because the denominator is close to zero.

Nonetheless, the main point is that beating occurs in this building as evidenced in Landers and Northridge records. This is important to note as such beating effects prolong the responses and therefore increase the number of large and small cycles of responses. Thus, even the increased number of smaller amplitude cycles become important due to possible low-cycle fatigue that can result in nonlinear behavior at joints.

CONCLUSIONS

This paper focused on analyses of acceleration and displacement responses recorded by 20-channels of accelerometers sparsely deployed at only seven levels of a 52-story building in downtown Los Angeles. To date, seven response data sets from seven earthquakes of different magnitudes and epicentral distances have been retrieved by CSMIP. Ambient data was not available. Using spectral analyses and system identification methods, translational and torsional frequencies for the lower four to five modes below 2 Hz are identified. Spectral analysis results in terms of amplitude spectra and ratios of amplitude spectra indicate that there is small or insignificant differences (1) of lower first four to five frequencies computed for each of the seven earthquakes and (2) in the fundamental frequencies for NS, EW, and torsional directions (~0.17 Hz) for all seven events. This indicates that translational and torsional modes are coupled. Furthermore, both amplitude spectra and ratios of amplitude spectra for the lower modes are very similar; hence structural responses are not affected by soil-structure interaction. It is noted that there is only one vertical accelerometer deployed right at the center of the imprint of the tower. This does not allow direct computation of rocking rotation of basement around a horizontal axis.

System identification methods N4SID and MOESP are applied to extract modal frequencies, modal damping and mode shapes for the first three modes in each direction. Torsional modes and their modal characteristics were also obtained. Critical damping percentages extracted from these methods are in general low (except for EW component of Northridge earthquake, which is higher, possibly due to computational and data quality anomalies).

Despite noisy and short data length and close modal frequencies of the building, several vibration modes of the building are successfully identified. For the particular data sets analyzed in this paper, results from both N4SID and MOESP algorithm applications compare well and are in general quite consistent.

The largest two responses of the building from Landers and Northridge earthquake infer that, in general, the computed critical damping percentages of the building particularly for the fundamental modes are small. Hence, it can be deduced that damping will be even smaller for ambient and smaller earthquake excited motions. However, damping percentages extracted for all seven earthquake data sets did not result in reliable correlation of damping percentages between the shaking level of the seven earthquakes. On the bright side, the general trend of lower damping percentages is consistent and important in analyses and design of tall buildings.

In addition, particularly for the Landers and Northridge earthquakes, the acceleration and displacement response data at the roof exhibits beating effect. As stated, beating occurs when fundamental translational and torsional periods are close and damping is low, which is the case for this building. The beating period, only visually observed from time history plots, vary between 80–130 s.

An important additional point needs to be made about the basin effect. The computed lowest frequency using basin data is ~ 0.12 Hz. This frequency is well within range of fundamental frequencies of taller buildings >50 or more stories. Therefore, future designs of tall buildings in downtown Los Angeles should consider the effect of possible low frequencies exhibited by computed basin transfer functions.

The structural frequencies obtained in this study using data set from seven earthquakes and application of spectral and system identification methods compare well with those computed by [Ventura and Ding \(2000\)](#) who performed (1) modal analyses after developing mathematical models and, also, (2) analyses of data from only two earthquakes (Sierra Madre and Northridge) using only spectral methods. They did not extract critical damping ratios. Our study resulted in a general trend of lower critical damping percentages, which is important for tall buildings. Lower damping percentages are also one important cause of beating effects, which of course can be mitigated by adding dampers within the structural system.

REFERENCES

- Abdelrazaq, A., 2012. Validating the structural behavior and response of Burj Khalifa: Synopsis of the full scale structural health monitoring programs, *International Journal of High-Rise Buildings* **1**, 37–51.
- Allemang, R. J., 2003. The modal assurance criterion – twenty years of use and abuse, *Journal of Sound and Vibration*, August, 14–21.
- Anderson, J. P., Bodin, P., Brune, J. N., Prince, J., Singh, S. K., Quass, R., and Onate, M., 1986. Strong ground motion from the Michoacan, Mexico, earthquake, *Science* **233**, 1043–1049.
- Bendat, J. S., and Piersol, A. G., 1980. *Engineering Applications of Correlation and Spectral Analysis*, John Wiley and Sons, New York, 472 pp.
- Boroschek, R. L., and Mahin, S. A., 1991. *Investigation of the Seismic Response of a Lightly Damped Torsionally Coupled Building*, Report UCB/EERC-91/18, Earthquake Engineering Research Center, University of California, Berkeley, 291 pp.

- Boroschek, R. L., Mahin, S. A., and Zeris, C. A., 1990. Seismic response and analytical modeling of three instrumented buildings, in *Proceedings, 4th U.S. National Conference on Earthquake Engineering*, Palm Springs, CA, vol. **2**, 219–228.
- Çelebi, M., Phan, L. T., and Marshall, R. D., 1993. Dynamic characteristics of five tall buildings during strong and low-amplitude motions, *Journal of The Structural Design of Tall Buildings* **2**, 1–15.
- Çelebi, M., 2004. Responses of a 14-story (Anchorage, Alaska) building to far-distance ($M_w = 7.9$) Denali Fault (2002) and near distance earthquakes in 2002, *Earthquake Spectra* **20**, 693–706.
- Çelebi, M., 2006. Recorded earthquake responses from the integrated seismic monitoring network of the Atwood Building, Anchorage, Alaska, *Earthquake Spectra* **22**, 847–864, November 2006.
- Çelebi, M., Prince, J., Dietel, C., Onate, M., and Chavez, G., 1987. The culprit in Mexico City – Amplifications of Motions, *Earthquake Spectra, Journal of EERI*, **3:2**. 315–328.
- Çelebi, M., Okawa, I., Kashima, T., Koyama, S., and Iiba, M., 2012. Response of a tall building far from the epicenter of the March 11, 2011 $M = 9.0$ Great East Japan earthquake and its aftershocks, paper no. 0291. *PROC. 15th WCEE*, Lisbon, Portugal, 24–28 September 2012.
- Çelebi, M., Okawa, I., Kashima, T., Koyama, S., and Iiba, M., 2014. Response of a tall building building far from the epicenter of the March 11, 2011 $M = 9.0$ Great East Japan earthquake and its aftershocks, *The Wiley Journal of the Structural Design of Tall and Special Buildings* **23**, 427–441, DOI:10.1002/tal.1047.
- Çelebi, M., Hisada, Y., Omrani, R., Ghahari, F., and Taciroglu, E., 2016a. Responses of two tall buildings in Tokyo, Japan, before, during, and after the $M9.0$ Tohoku Earthquake of 11 March 2011. *Earthquake Spectra* **32**, 463–495.
- Çelebi, M., Kashima, T., Ghahari, S. F., Abazarsa, F., and Taciroglu, E., 2016b. Responses of a tall building with US code-type instrumentation in Tokyo, Japan - to events before, during and after the Tohoku earthquake of March 11, 2011. *Earthquake Spectra* **32**, 497–522.
- Haskell, N. A., 1953. The dispersion of surface waves on multi-layered media, *Bull. Seismological Soc. Am.* **43**, 17–34.
- Haskell, N. A., 1960. Crustal reflection of plane SH waves, *J. Geophysical Res.* **65**, 4147–4150.
- Hillhouse, J. W., Reichard, E. G., and Ponti, D. J., 2002. *Probing the Los Angeles Basin—Insights Into Ground-Water Resources and Earthquake Hazards*, USGS Fact Sheet 086-02, 2 pp., available at <http://geopubs.wr.usgs.gov/fact-sheet/fs086-02/>.
- Hodgson, J. J., 1964. *Earthquakes and Earth Structure*, Prentice-Hall, Englewood Cliffs, NJ.
- Juang, J. N., 1994. *Applied System Identification*, Prentice Hall, Upper Saddle River, NJ, 394 pp.
- Kubo, T., Hisada, Y., Murakami, M., Kosuge, F., and Hamano, K., 2011. Application of an earthquake early warning system and a real-time strong motion monitoring system in emergency response in a high-rise building, *Soil Dynamics and Earthquake Engineering* **31**, 231–239.
- Ljung, L., 1987. *System Identification: Theory and User*, Prentice Hall, Englewood Cliffs, NJ.
- Mathworks, 2013 and previous versions. *Matlab and Toolboxes*, South Natick, MA.
- Nakata, N., Snieder, R., Kuroda, S., Ito, S., Aizawa, T., and Kunimi, T., 2013. Monitoring a Building using deconvolution interferometry. I: Earthquake-data analysis, *Bull. Seismol. Soc. Am.*, **103**, 1662–1678.

- Nakata, N., Snieder, R., and S., 2014. Monitoring a building using deconvolution interferometry. II: Ambient-vibration analysis, *Bull. Seismol. Soc. Am.*, **104**, 204–213.
- Rahmani, M., and Todorovska, M. I., 2014. 1D system identification of a 54-story steel frame building by seismic interferometry, *Earthquake Eng. and Structural Dynamics* **43**, 627–640.
- Rahmani, M., and Todorovska, M., 2015. Structural health monitoring of a 54-story steel frame building using wave method and earthquake records, *Earthquake Spectra* **31**, 501–525.
- Snieder, R., and Safak, E., 2006. Extracting the building response using seismic interferometry: Theory and application to the Millikan Library in Pasadena, California, *Bull. Seismol. Soc. Am.* **96**, 586–598.
- Süss, M. P., and Shaw, J. H., 2003. P-wave seismic velocity structure derived from sonic logs and industry reflection data in the Los Angeles Basin, California, *J. Geophysical Res.* **108/B3**, 2170, pp. ESE 13-1–13-18, DOI:10.1029/2001JB001628.
- Tezcan, S. S., and Ipek, M., 1972. Long distance effects of the 29 March 1970 Gediz, Turkey, earthquake, *Earthquake Engineering and Structural Dynamics* **1**, 203–215.
- Ulusoy, H. S., Feng, M. Q., and Fanning, P. J., 2011. System identification of a building from multiple seismic records, *Earthquake Engineering and Structural Dynamics* **40**, 661–674.
- Van Overschee, P., and De Moor, B., 1996. *Subspace Identification for Linear Systems*, Kluwer Academic Publishers, Dordrecht, The Netherlands.
- Van Overschee, P. V., and De Moor, P., 1995. A unifying theorem for three subspace system identification algorithms, *Automatica* **31**, 1853–1864.
- Van Overschee, P. V., and De Moor, P., 1994. N4SID: Subspace algorithms for the identification of combined deterministic-stochastic systems, *Automatica* **30**, 75–93.
- Ventura, C., and Ding, Y., 2000. Linear and nonlinear seismic response of a 52-storey steel frame building, *Journal of The Structural Design of Tall Buildings* **9**, 25–45.
- Verhaegen, M., 1994. Identification of the deterministic part of mimo state space models given in innovations form from input–output data, *Automatica* **30**, 61–74.
- Viberg, M., 1995. Subspace-based methods for the identification of linear time- invariant systems, *Automatica* **31**, 1835–1851.

(Received 5 May 2015; accepted 4 November 2015)